THE JOURNAL OF PHYSICAL CHEMISTRY C
A JOURNAL OF THE AMERICAN CHEMICAL SOCIETY

pubs.acs.org/JPCC

Article

Theoretical Study on the Nitrogen Reduction Reaction (NRR) on Cu Oxide-Based Electrocatalysts

Published as part of The Journal of Physical Chemistry C special issue "Degradation of Electrochemical Materials in Energy Conversion and Storage."

Stefanie E. Bogenrieder,[‖] C. Hepsibah Priyadarshini,[‖] Julian Beßner, and Timo Jacob*

Cite This: *J. Phys. Chem. C* 2025, 129, 15978–15990

Read Online

ACCESS | Metrics & More | Article Recommendations | Supporting Information

ABSTRACT: Inspired by the excellent carrier concentration and escalated catalytic activity of CuO, the reduction of N_2 to NH_3 was studied using density functional theory. Concentrating on the most stable CuO(111) surface orientation, different surface terminations as well as defective surfaces were considered. Analyzing the free energies involved in nitrogen reduction reaction (NRR) across different pathways based on the associative Heyrovský mechanism highlights the reconstructed Cu-terminated and O-defective surfaces to be the prospective ones, with *NNH formation free energies of 1.41 and 1.45 eV, significantly lower than 2.58 eV observed for the pristine surface. However, the preferential mechanism on the reconstructed surface is characterized by endergonic hydrogenation steps, whereas for the O-defective surface, all steps are downhill and exergonic. Subsequently, the negative free energy for the desorption of NH_3 from the O-defective surface discloses the availability of catalytic sites for further NRR. In addition, the reconstructed surface possessing multifarious coordinatively unsaturated Cu atoms succumbs to irreversible structural variations, unlike the O-defective surface, which has well-defined active centers. Moreover, Bader charge and charge density difference analyses showcase extensive hybridization between the Cu−3*d* and N−2*p* states on the O-defective surface. Further, the highest ICOHP value of −15.15 recorded for the O-defective surface displayed a significant activation of the N≡N triple bond in N_2, which corroborates the enhanced catalytic activity of the O-deficient surface.

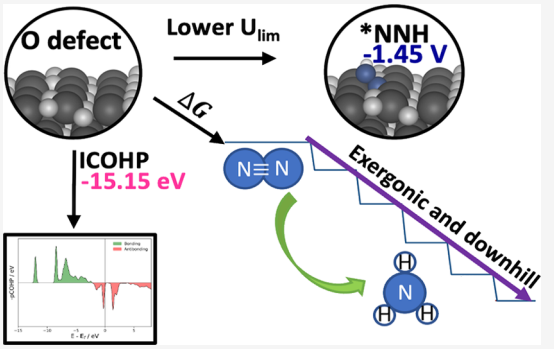

INTRODUCTION

Almost 80% of the ammonia produced in the world is responsible for sustaining 7.9 billion people by acting as one of the crucial fertilizers, and the remaining fraction is utilized in various industries that manufacture explosives, textiles, petroleum, or leather. Conventionally, NH_3 is manufactured by the Haber−Bosch process, which requires extreme conditions of temperature (600−800 K) and pressure (150−250 atm). However, this production contributes to 2 and 3% of the world's total energy consumption and greenhouse gas generation, thereby raising serious environmental concerns.[1−3] Furthermore, ammonia is currently also considered as a prospective energy carrier for a potential hydrogen-based energy economy. Thus, electrocatalytic NRR under ambient conditions is believed to be one of the sustainable strategies for NH_3 production. In general, noble metal electrocatalysts such as Ag, Ru, and Au have proven to be outstanding in terms of exhibiting enhanced selectivity and commendable activity.[4−6] Conversely, their usability is greatly hindered owing to their scarcity and expensive nature. Hence, the scientific community has been working toward the development of stable, selective, and cost-effective electrocatalysts that can bring down global energy consumption as well as carbon emissions. Among various materials, metal oxides are held in high regard owing to their synthesizability, unique electronic properties, high stability, minimal energy consumption, moderate faradaic efficiency, as well as tunable activity. They are known to accelerate catalytic efficiency in hydrogen evolution reaction (HER), CO_2 reduction reaction (CO_2RR), oxygen evolution reaction (OER), as well as nitrogen reduction reaction (NRR).[7−10]

In that, CuO has garnered increasing attention owing to its excellent charge carrier concentration (holes and electrons from Cu and O vacancies as well as coupling between charge carriers resulting in polarons), configurable band gap,

Received: May 28, 2025
Revised: August 17, 2025
Accepted: August 18, 2025
Published: September 2, 2025

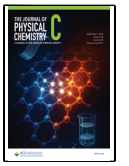

https://doi.org/10.1021/acs.jpcc.5c03667
J. Phys. Chem. C 2025, 129, 15978−15990

enhanced catalytic activity, and long-term durability at higher temperatures. Thus, it finds applications in fields including but not limited to gas sensors, batteries, photocatalysis, supercapacitors, and electrocatalysis.[11−16] Besides, Jang *et al.* explored the role of Cu_2O and CuO as photocathodes for photochemical NRR. In that, a faradaic efficiency of 20 and 17% has been observed for Cu_2O and CuO at 0.4 and 0.6 V *vs* HER, respectively.[17] Interestingly, for hydrogen evolution, CuO showcased a negligible faradaic efficiency of 0.5%. Thus, CuO favors the formation of ammonia rather than hydrogen. However, this cathode showed limited stability due to cathodic corrosion via the reduction of Cu^{2+} by photoexcited electrons.[17] In addition, Wang *et al.* studied electrocatalytic NRR on CuO surfaces both experimentally and computationally.[18] Here, the current density was found to be constant for 8000 s under different potentials, demonstrating the CuO surface to be an excellent candidate for electrocatalytic reduction of N_2 to NH_3.[18]

In general, chemisorption of reactants at (or near) the catalyst's active sites, followed by subsequent activation mediated by electron transfer processes, provides a pathway with lower free energy barriers.[19] Thus, the primary challenge in the NRR is to surmount the large energy barrier associated with the reduction of N_2. However, the inertness of N_2 brought about by a synergetic effect of escalated N≡N bonding energy, non-polarity, negative electron affinity, as well as large ionization energy, effectuate higher overpotential and lower faradaic efficiency.[19] Hence, to gain more detailed insights and to elaborate on these bottlenecks, we have examined the electrocatalytic activity of polar stoichiometric and non-stoichiometric CuO surfaces for NRR. Interestingly, the electronic properties of these metal oxides span between metallic and semiconducting zones which can be exploited for designing advanced functional materials.[20] Besides, the physical and chemical properties of bulk structures deviate from these constructed nanostructured surfaces, which often contain unsaturated sites and undergo local reconstructions that have the potential to aid the activation of the inert N≡N triple bond. Thus, a thorough understanding of the custom-made CuO nanostructures at the molecular level is mandatory and has been realized in our previous work.[21]

Building on our previous study on the stability and properties of different Cu oxides, in this work, we explore the details of the NRR on different CuO(111) surfaces, either having mixed surface terminations, being reconstructed, or having surface defects.[22] Thus, this comprehensive study provides a detailed understanding of the influence of polar stoichiometric and nonstoichiometric surfaces as electrocatalysts from structural, thermodynamic, and electronic viewpoints. Furthermore, this research article will furnish answers to important questions, including: (i) what are the preferential sites on CuO(111) for the nitrogen reduction reactions; (ii) which mechanism is thermodynamically favored for diverse CuO surfaces; (iii) what is the effect of monatomic defects on the reaction; and (iv) which is the most promising CuO(111) surface for NRR?

COMPUTATIONAL DETAILS

The Vienna *ab initio* Simulation Package (VASP) was utilized to perform all calculations in the present study.[23,24] Here, the projector-augmented wave (PAW) method was employed to address the interactions persisting between core electrons and nuclei.[25] Moreover, the exchange−correlation functional developed by Perdew, Burke, and Ernzerhof (PBE) was adopted.[26] In addition, the 3*d* states of Cu in CuO were treated with the Hubbard correction (DFT+*U*) established by Dudarev *et al.* in order to reduce the self-interaction errors.[27] The detailed information pertaining to the choice of the Hubbard correction value of 8 eV for the 3*d*-states in CuO has been meticulously corroborated in our previous article and is found to align with the *U* values documented in literature.[21,28]

CuO(111):Cu/O, CuO(111):Cu, as well as monatomic O- and Cu-defective CuO(111):Cu/O surfaces were modeled with a 2 × 2 supercell, comprising three oxide layers. A vacuum of 20 Å was added in the direction perpendicular to the surface to avoid spurious interactions of the slab with its periodic images. Also, the two topmost layers and the adsorbates were allowed to freely relax, whereas constraints were placed on the bottom layer in order to simulate bulk behavior. These structural settings are equivalent to the set of parameters utilized in our previous study on bulk Cu oxides of various surface orientations.[21] In addition, a force convergence criterion of 10^{-2} eV/Å and a ***k***−point grid of 3 × 3 × 1 were utilized. Moreover, denser Monkhorst−Pack ***k***−point grids of 7 × 7 × 1 were adopted for evaluating the projected density of states (PDOS).

In general, the energy required for the adsorption of nitrogen over the above-mentioned surfaces (E_{ad}) can be estimated by the following equation

$$E_{ad} = E_{S+N} - \left(E_S - \frac{1}{2}E_{N_2}\right) \quad (1)$$

where E_{S+N} and E_S denote the energies of nitrogen adsorbed on the surface and the clean surface, respectively, whereas E_{N_2} is the energy of an N_2 molecule in the gas phase. Likewise, the change in free energy (ΔG) for the intermediates of the NRR at the room temperature (298 K) has been evaluated based on the computational hydrogen electrode (CHE) model proposed by Nørskov *et al.*[29] as follows:

$$\Delta G = \Delta E + \Delta E_{ZPE} - T\Delta S - n{\cdot}eU \quad (2)$$

where ΔE is the reaction energy corresponding to the total energies estimated from DFT, while ΔE_{ZPE} and ΔS describe variations in zero-point energy and entropy. Also, n represents the number of transferred electrons, and U indicates the bias potential. For gas-phase nitrogen, the experimental standard enthalpy of NH_3 was taken as reference, as suggested by Urrego-Ortiz *et al.*[30,31] Subsequently, frequency analysis was performed in order to gauge entropy contributions and ZPE of the adsorbed intermediates, whereas ΔS values for the molecules in gaseous phases were extracted from thermodynamic data documented in the NIST database.[32] All formation energies are referenced to bulk Cu as well as half of the molecular oxygen, nitrogen, and hydrogen.

In addition, the limiting potential (U_{lim}) refers to the bias potential at which all of the elemental reaction steps are exothermic. For an accurate determination of U_{lim}, the change in free energy of the potential-determining step (ΔG_{PDS}) is considered:

$$U_{lim} = \frac{-\Delta G_{PDS}}{n{\cdot}e} \quad (3)$$

In addition, Bader charges and integrated crystal Hamilton population (ICOHP) analyses were performed for NRR

https://doi.org/10.1021/acs.jpcc.5c03667
J. Phys. Chem. C 2025, 129, 15978−15990

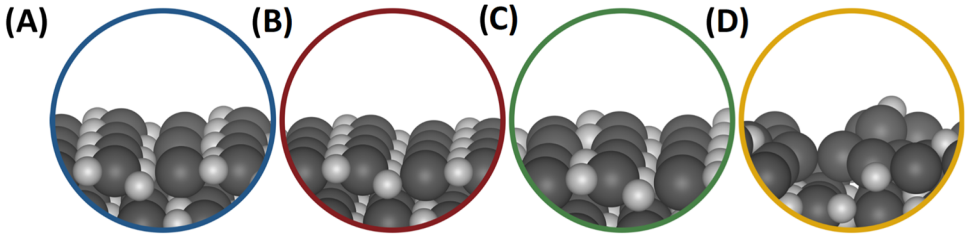

Figure 1. Surface structures of (A) pristine CuO(111):Cu/O, (B) CuO(111): Cu, (C) O-defective, and (D) Cu-deficient CuO(111):Cu/O surfaces.

Scheme 1. Schematic Representation of the Steps Involved in NRR for the Scrutinized Reaction Pathways: The Different Reduction Mechanisms, Including Alternating, Distal, Enzymatic, and Enzymatic$_{var}$ Are Displayed in Green, Orange, Blue, and Yellow, Respectively

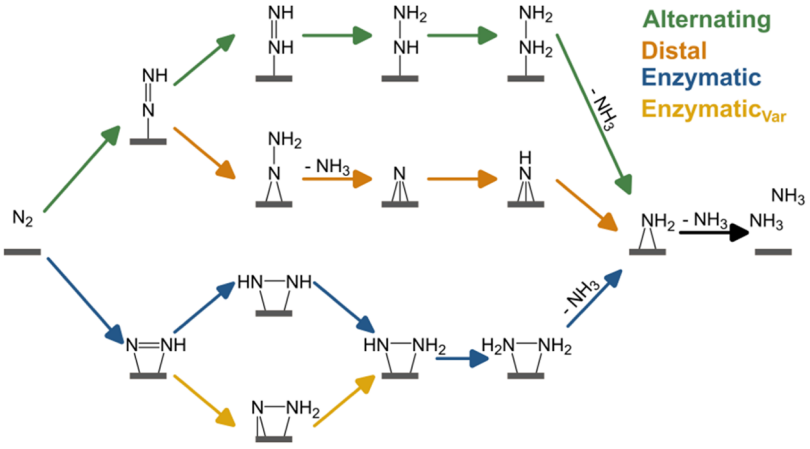

intermediates of interest to gauge the charges transferred and the bond strength, respectively.[33−35]

RESULTS AND DISCUSSION

Scrutinization of the Catalyst Surface for NRR. Determining the surface structure that is stable under reaction conditions plays an important role in facilitating the adsorption and activation of N_2 for NRR. Hence, in our previous work, the stability of various surfaces has been evaluated, and among the investigated CuO(111) structures, the stoichiometrically terminated CuO(111):Cu/O surface revealed an exceeding thermodynamic stability over the entire range of oxygen chemical potentials.[21] This evaluation is in excellent agreement with the results obtained by Mishra *et al.* and Hu *et al.*[20,36] Thus, this surface orientation was used for our studies of the NRR mechanism. In addition, we have also explored the NRR mechanism on the Cu-terminated, monatomic O- and Cu-defective CuO(111):Cu/O surface, respectively (cf. Figure 1).

Adsorption of Atomic N. As an initial step, we have studied the adsorption of atomic nitrogen on CuO(111):Cu/O. Twelve plausible positions were considered, based on the coordination number and magnetic moment (see Figure S1). Besides, the binding energies of the structures, along with their bond lengths, are furnished in Table S1. In the case of structures A and B, incorporation of N on top of the coordinatively unsaturated Cu atom ($Cu_{3K\pm}$) resulted in Cu−N bond lengths of 1.81 and 1.80 Å, respectively, with relatively diminished stability (cf. Figure S1A and Table S1). Here, indices 3K/4K correspond to the coordination number, and ± values indicate the sign of the magnetic moment of the surface Cu atom. Moreover, least stable configurations with binding energies of −0.04 and −0.08 eV were recorded for the adsorbate relaxed on top of the coordinatively saturated Cu atom ($Cu_{4K\pm}$) in structures C and D. This can be ascribed to the enlarged Cu−N bond length of 2.34 Å when compared to the one observed for N adsorbed at $Cu_{3K\pm}$ sites (∼1.8 Å). Thus, this behavior clearly revealed that N adsorption preferentially takes place on electron-deficient sites with unoccupied *d*-orbitals rather than at completely saturated sites. However, when N was placed in between Cu ($Cu_{3K\pm}$ or $Cu_{4K\pm}$) and O ($O_{3K\pm}$ or $O_{4K\pm}$) in the case of structures E−L, it was observed that adsorbates engaging in a tridentate configuration with one O and two Cu atom(s) led to a surge in stability. Interestingly, atomic N between $Cu_{4K\pm}$ and O_{3K+} atoms, resulting in a similar tridentate configuration, yielded the lowest binding energy of −3.10 eV (cf. Figure S1J and Table S1). Although the magnetic properties of the surface influence the adsorption behavior of nitrogen on CuO(111):Cu/O, its impact is comparatively smaller ($\Delta E_{ads} = E_{ads}$ (A) $- E_{ads}$(B) = 0.04 eV) than that of the coordination environment ($\Delta E_{ads} = E_{ads}(C) - E_{ads}$(J) = 3.06 eV). Hence, the following discussion will only emphasize the effect of the coordination environment in analyzing adsorbate−surface interactions.

Exploration of Reaction Pathways for NRR on CuO(111):Cu/O. In general, mechanisms facilitating nitrogen reduction reactions are classified as associative and dissociative, respectively. As the initial N_2 dissociation along the dissociative pathway is rather energy demanding, in the current study, we concentrated solely on the associative Heyrovský mechanism.[37] Overall, the nitrogen reduction reaction is characterized by six coupled proton and electron transfer steps. Based

https://doi.org/10.1021/acs.jpcc.5c03667
J. Phys. Chem. C 2025, 129, 15978−15990

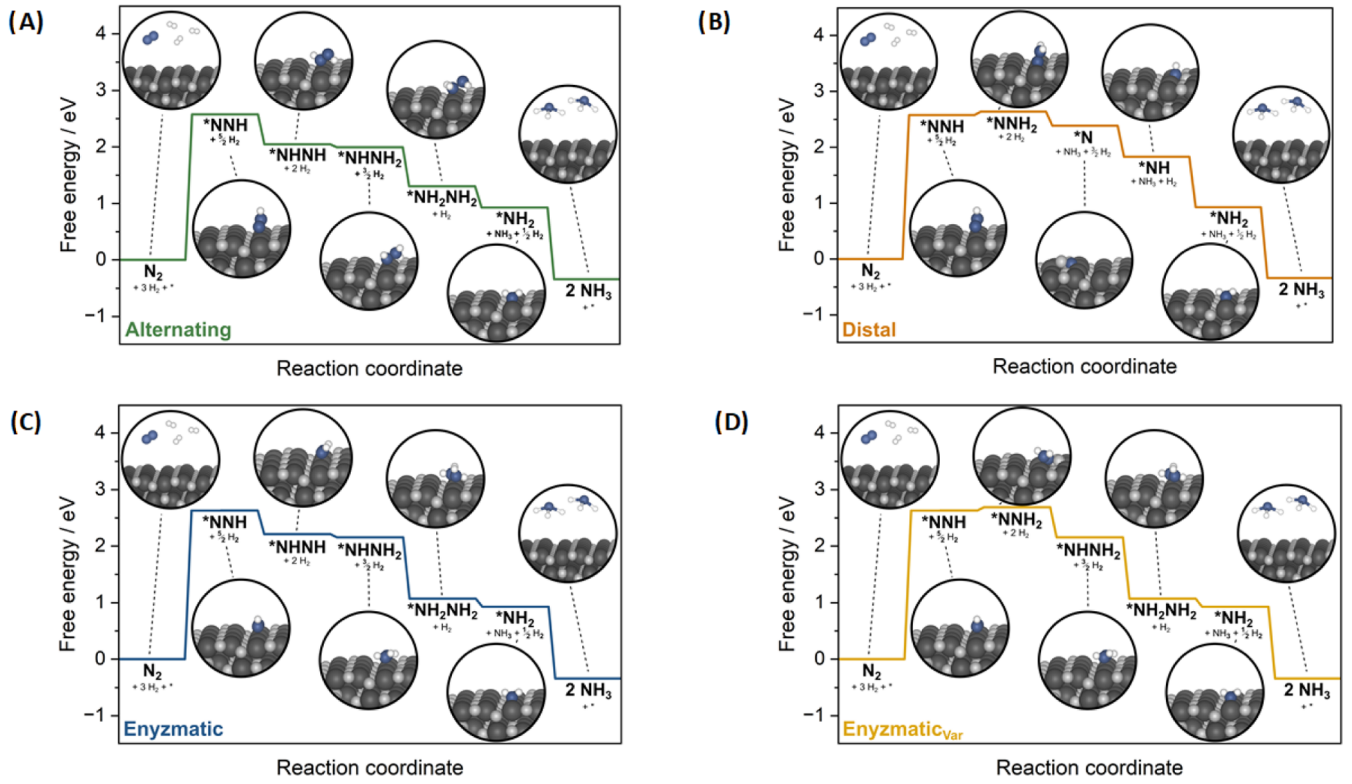

Figure 2. Free energy diagrams of (A) alternating, (B) distal, (C) enzymatic, and (D) enzymatic$_{var.}$ mechanisms depicting the individual steps along with the associated structures involved in the reduction of N_2 to NH_3 on CuO(111):Cu/O. In the hard-sphere models, the white, blue, and light and dark gray spheres correspond to hydrogen, nitrogen, oxygen, and copper atoms, respectively.

on this sequence, the associative pathway can be further categorized into alternating, distal, enzymatic, and enzymatic variation (enzymatic$_{var.}$) (cf. Scheme 1).

Similar to the adsorption of atomic nitrogen on CuO(111):Cu/O, the adsorption of all of the other NRR intermediates has been scrutinized and detailed in the following section. In order to simulate the adsorption of polyatomic intermediates, the intermediates were subjected to rotations, and the suitability of the resulting configurations was evaluated in all plausible positions on CuO(111):Cu/O. Further, the course of the free energy profiles (using eq 2) for diverse NRR mechanisms displayed in Scheme 1 was analyzed, considering the most stable adsorption structure for each intermediate. The resulting free energy diagrams, in tandem with the corresponding structures, are showcased in Figure 1A–D.

The adsorption pattern of various intermediates formed along the reduction of nitrogen via the alternating pathway is shown in Figure 2A. As expected, the initial step of transforming stable N_2 to *NNH requires the highest energy, owing to the extremely strong and inert nature of N≡N. The free energy of this endergonic process amounts to 2.58 eV, revealing that it is thermodynamically less favored. However, from the second consecutive H addition, the free energy decreases continuously until the final formation of NH_3. In the case of the *NH_2 intermediate, it can be seen that a bridge position between two Cu_{3K} atoms with Cu–N bonds of around 2 Å each is energetically preferred. Besides, continuous increments in N–N bond lengths from 1.11 (for the N_2 molecule) to 1.18, 1.24, 1.33, and 1.47 Å for *NNH, *HNNH, *HNNH_2, and *NH_2NH_2 intermediates signify the ease with which the bond between two nitrogen atoms can be broken in order to facilitate the release of NH_3. This increasing trend in bond lengths demonstrates that the CuO(111):Cu/O surface might indeed enhance the activation of molecular N_2. Moreover, the final step of nitrogen reduction yielded ammonia with higher negative free energies, signifying the spontaneity of the process.

Along the distal mechanism, five catalytic intermediates, including *NNH, *NNH_2, *N, *NH, and *NH_2, can be distinguished (cf. Figure 2B). Initially, the distal N atom was constantly hydrogenated by the proton–electron pair until the breaking of the N≡N bond, thereby resulting in the release of the first ammonia molecule. Consequently, hydrogenation of the atomic N bound to the surface effectuated the release of the second NH_3 molecule. Similar to the results observed for the alternating mechanism, from a thermodynamic perspective, the first hydrogenation step along the distal mechanism is also limiting. Subsequently, the second step is also found to be higher in energy. Here, the *NNH intermediate preferentially adsorbs between two Cu_{3K} surface atoms, each of which results in a Cu–N bond. The bond lengths between N atoms for the first and second intermediates were 1.20 and 1.25 Å, respectively. In the third reduction step, the adsorption of the single N atom again establishes a tridentate contact with two Cu atoms and one O. This finding aligns with the insights on N bonding presented in the previous section. In contrast to the first and second hydrogenation steps, the remaining steps revealed a decrease in free energy with the incorporation of additional H atoms. Furthermore, the last reduction step is found to be thermodynamically favored with a more negative free energy.

Considering the enzymatic mechanism, the first hydrogenation step is found to be endergonic with the highest free

https://doi.org/10.1021/acs.jpcc.5c03667
J. Phys. Chem. C 2025, 129, 15978–15990

energy of 2.63 eV (cf., Figure 2C). The intermediates, including *NHNH, *$NHNH_2$, and *NH_2NH_2, with both of their N atoms attached to one Cu (Cu_{3K}) atom, were found to be very stable. Also, the bond lengths between the two N atoms surge from 1.11 to 1.20, 1.26, 1.38, and 1.44 Å, thereby facilitating the breakage of the first ammonia unit. Consecutively, with further addition of hydrogen, the second NH_3 molecule desorbs from the surface, recording higher negative energies.

Analyzing the free energy profile along the enzymatic$_{var}$ mechanism, it becomes clear that the initial hydrogenation process is thermodynamically demanding, with a required energy of 2.63 eV. Also, the second hydrogenation step, resulting in *NNH_2 intermediate, required a slightly higher energy than the former one (cf. Figure 2D). In all of the mechanisms, the free energy corresponding to NH_3 desorption from the CuO(111):Cu/O surface is negative, implying the availability of catalytic sites for further N_2 adsorption.

Further, the free energy profiles evaluated above are collectively displayed in Figure 3 to facilitate the comparison

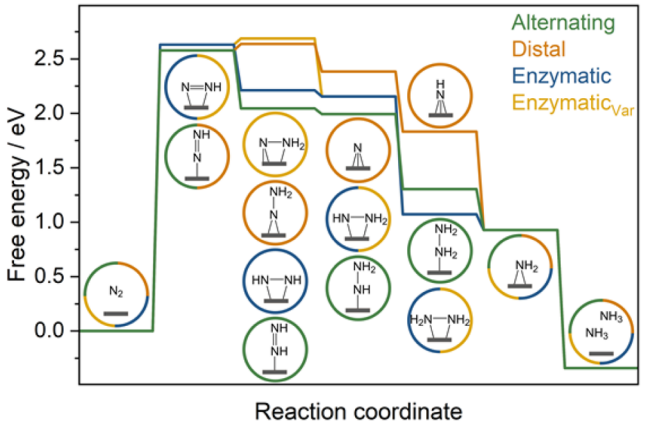

Figure 3. Combined free energy plots for various mechanisms scrutinized for the NRR in the CuO(111):Cu/O surface. The schematic representation of alternating, distal, enzymatic, and enzymatic$_{var.}$ intermediates are given in green, orange, blue, and yellow color circles, respectively. Intermediates that can commonly be assigned to diverse pathways are indicated via circles with multiple colors.

of different pathways for NRR on CuO(111):Cu/O. Figure 3 illustrates that, for the first reduction step, one of the N atoms attached to a surface Cu atom along the alternating and distal mechanisms is energetically more stable by 0.05 eV than the configuration in which both N atoms are bound to the surface, as seen along the enzymatic and enzymatic$_{var.}$ pathways. Considering the second step, it can be evidenced that the intermediates obtained via the alternating and enzymatic pathways are the most stable ones, respectively. Thus, the second H atom prefers binding to the other N atom (alternating and enzymatic) rather than to the same (distal and enzymatic$_{var.}$).

For the third reduction reaction, the *NHNH intermediate of the alternating mechanism appeared to be the most favorable one. However, for the fourth hydrogenation step, the *NH_2NH_2 intermediate of the enzymatic mechanism, which is doubly bound to two surface Cu atoms, is preferent. Interestingly, a thermodynamically feasible mixed pathway where the NRR can proceed by switching between alternating, distal, enzymatic, and enzymatic$_{var.}$ mechanisms based on the energetically preferent intermediates of the individual hydrogenation steps has been derived for the CuO(111):Cu/O surface, as depicted in Figure 4. With an exception in the formation of *NH_2NH_2, where both N atoms are linked to two surface Cu atoms, the alternating pathway dominated. This finding aligns well with the DFT study of NRR carried out on CuO(111) by Wang *et al.*[18] that indicated the preference of an alternating mechanism for the reduction of N_2. Similarly, the initial hydrogenation of N_2 to *NNH emerged as the energy-intensive step for the overall reaction with a limiting potential of −2.58 V (cf. Figure S2A).

It should be noted that the low Gibbs free energies observed for interactions of gaseous N_2 and NH_3 molecules with the catalyst surface conspicuously showcase their ease of desorption.[38−40] Thus, these species might adsorb as metastable intermediates that could indeed slightly reduce the activation energy of the subsequent reaction step. However, the chemical activity of the catalyst is low to activate N_2, for instance, the application of a plasma might accelerate the interaction between these two entities.[41−45]

NRR on Cu-Terminated Surfaces. In the case of reducing conditions, there is a decrease in the number of oxygen atoms on CuO(111). Under these conditions, the surface phase diagram reveals the Cu−terminated CuO(111) surface, *i.e.*, CuO(111):Cu, to be most relevant.[21] Here, the surface oxygen atoms coordinated to four Cu atoms, as in bulk, are coordinatively saturated, whereas a few Cu atoms in the topmost surface layer are linked to two O atoms and coordinatively unsaturated (cf. Figure 5). Meanwhile, Cu

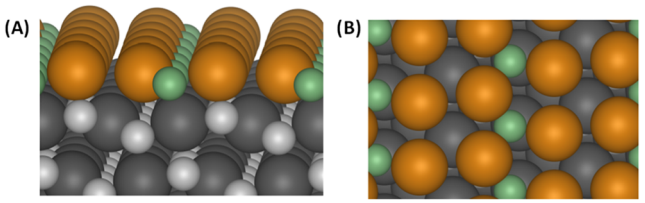

Figure 5. (A) Side and (B) top views of the optimized CuO(111):Cu surface. The larger and smaller spheres denote Cu and O atoms, respectively. In the coordination environment, the orange and green-colored spheres represent atoms with coordination numbers (CN) two and four, correspondingly.

atoms bound to different numbers of O atoms result in distinct coordination environments on this surface. In addition, Bader charge analyses revealed that charges on Cu atoms with respect to the coordination environment were 0.4 and 0.5 e. This indicated that Cu atoms have undergone a reduction from the

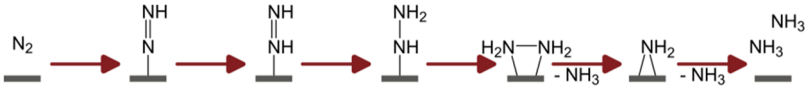

Figure 4. Schematic representation of the thermodynamically feasible mixed pathway for NRR on the CuO(111):Cu/O surface.

https://doi.org/10.1021/acs.jpcc.5c03667
J. Phys. Chem. C 2025, 129, 15978−15990

+2 to +1 state, which is in accordance with the corresponding literature.[21] Further, based on the coordination environment, a few Cu atoms recorded a magnetic moment of −0.2 μ_B or none at all. Subsequently, the adsorption of NRR intermediates, as displayed in Scheme 1, has been meticulously tested on and between the distinguishable surface atoms of CuO(111):Cu.

Contrary to CuO(111):Cu/O, the adsorption of NRR intermediates on CuO(111):Cu led to an irreversible reconstruction of the surface. Also, distinct rearrangements of the surface atoms with respect to the nature and adsorption position of the intermediates were observed. As displayed in Figure 6, the adsorption position of *NNH on CuO(111):Cu

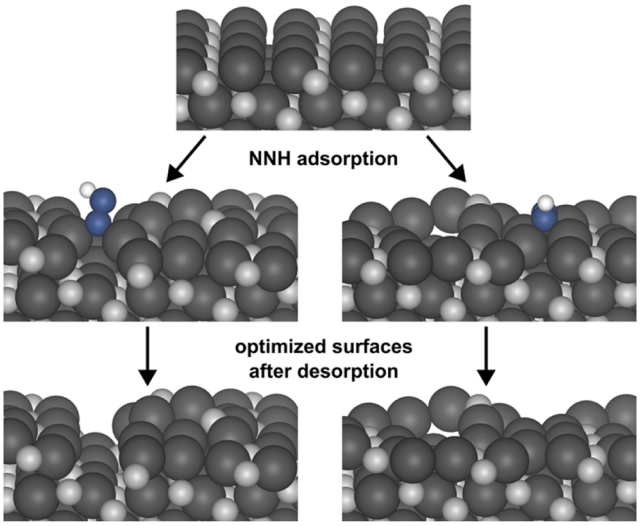

Figure 6. Structural representation of reconstructions effectuated by adsorption of *NNH intermediates in the CuO(111):Cu surface. The images at the top, center, and bottom zones signify surfaces before and during adsorption of *NNH intermediate (shown with respect to two different positions on the surface) as well as after desorption.

effectuated various changes in the surface structure. In addition, the removal of adsorbates, followed by geometry optimization, resulted in reconstructed surfaces rather than the original unreconstructed surface. This can be cognized from Figure 6, where the desorption of *NNH intermediate from two plausible sites yielded a reconstructed surface, whose energy varied from the unreconstructed one by −4.68 and −2.66 eV.

Hence, it becomes conspicuous that the CuO(111):Cu surface exists in a metastable state, while the adsorption and desorption of NRR intermediates facilitate the transformation to thermodynamically more stable surface morphologies. These differences in energy signified the existence of several local minima for the unreconstructed surface and thus pose a significant challenge in estimating the energy profile for NRR. Therefore, based on the thorough evaluation of adsorbates on CuO(111):Cu, an energetically preferent reconstructed surface, which differed from the unreconstructed one by −5.48 eV, was selected for further calculations (cf. Figure 7).

Determination of NRR on Reconstructed CuO(111):Cu. Unlike CuO(111):Cu, the atoms of the reconstructed surface do not follow a regular pattern in their arrangement. Instead, there are groups of atoms existing in a specific arrangement, thereby offering a diverse coordination environment for Cu and O atoms. The coordination number

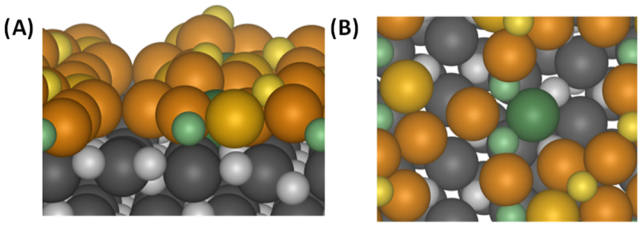

Figure 7. (A) Side and (B) top views of the relaxed reconstructed CuO(111):Cu surface. The larger and smaller spheres represent the Cu and the O atoms. In accordance with the coordination environment, the surface atoms are exhibited as orange (CN = 2), yellow (CN = 3), and green (CN = 4)-colored spheres, respectively.

of O decreases after relaxation, whereas the average coordination number of the Cu atom increases. Besides, two-coordinated Cu atoms of the reconstructed surface adopt an almost linear O−Cu−O arrangement as prevalent in the Cu_2O bulk phase. The Bader charges estimated for the doubly coordinated Cu atoms of the unreconstructed surface amounted to 0.4 and 0.5 e. These values corroborated the existence of doubly coordinated Cu atoms in a reduced state (Cu^+) by aligning with the charges estimated for Cu^+ in Cu_2O.[21] In addition to the rearrangement of atoms in the topmost surface layer, a reorganization of atoms in the second surface layer is also observed.

In the next step, the NRR was scrutinized on the reconstructed CuO(111):Cu surface, and the corresponding energy diagrams together with the structures are displayed in Figure S3A−D. It can be evidenced from all four mechanisms that the hydrogenation of N_2 to *NNH serves as the limiting step of nitrogen reduction to NH_3. However, the change in free energy for this hydrogenation step on the reconstructed CuO(111):Cu surface is lower by 1.41 and 1.48 eV when compared to the corresponding mechanisms on CuO(111):Cu/O. This can be attributed to the stronger adsorption on the reconstructed CuO(111):Cu surface, which greatly stabilizes the structure, explaining the increased stabilization of NRR intermediates on the reconstructed surface when compared to the CuO(111):Cu/O surface.

In order to compare the various pathways via which the reduction of N_2 takes place on the reconstructed surface, the corresponding energy profile is exhibited in Figure 8. Contrary to the CuO(111):Cu/O surface, the adsorption of *NNH, as

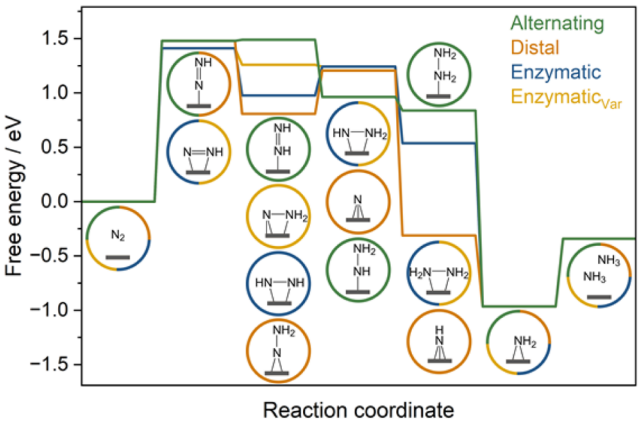

Figure 8. Combined free energy profiles for different pathways examined for NRR on reconstructed CuO(111):Cu.

https://doi.org/10.1021/acs.jpcc.5c03667
J. Phys. Chem. C 2025, 129, 15978−15990

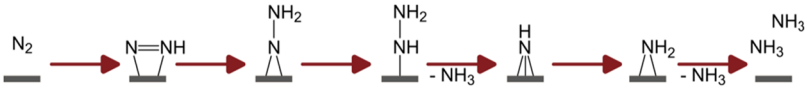

Figure 9. Schematic representation of the thermodynamically favored intermediates involved in the reduction of N_2 to NH_3 via a mixed pathway on CuO(111):Cu reconstructed surface.

described by the enzymatic and enzymatic$_{var.}$ mechanisms with both N atoms attached to one Cu atom each, is highly preferred on the reconstructed CuO(111):Cu surface. The difference in energies between the singly and doubly bound N to Cu atoms in *NNH amounts to 0.07 eV. Consecutively, the attachment of a second hydrogen atom to the same as the first N atom is preferred for the second hydrogenation step. Hence, the distal mechanism is favored over the alternating mechanism for the reconstructed surface. Besides, the intermediate of the alternating mechanism is the least stable, which is in contrast to that observed for CuO(111):Cu/O. Similar to the third reduction step on CuO(111):Cu/O, the singly bound *$NHNH_2$ intermediate of the alternating mechanism is favored. For the fourth hydrogenation step, the *NH intermediate of the distal mechanism is significantly stabilized by the reconstructed surface, where one NH_3 molecule splits off. Also, the largest free energy change of −1.27 eV was noticed between the third (*NH_2NH) and fourth (*NH) hydrogenation fractions. However, the adsorption of the *NH_2 intermediate is more stable than the generation of the NH_3 molecule. Furthermore, the initial, third, and final reduction steps are endergonic in nature, whereas the remaining ones are all exergonic. The thermodynamically favorable pathway for NRR on the reconstructed CuO(111):Cu surface is a combination of enzymatic, distal, and alternating mechanisms, where the distal pathway plays a preponderant role. Besides, NRR along this pathway requires a limiting potential of −1.41 V (cf. Figure S2B).

Similar to CuO(111):Cu/O, the thermodynamically feasible mixed mechanism derived from energetically favorable intermediates of the plausible pathways has been furnished in Figure 9.

Influence of Monatomic Defects on the NRR on CuO(111):Cu/O. In general, tailoring defects to enhance electrochemical reactions, including the OER, HER, ORR, and CO_2RR, has garnered much attraction. Unlike the defect-free surface, the one with vacancies exhibits great potential in altering the electronic structure in addition to creating new active sites that are extremely vital for electrocatalytic reactions by offering escalated activity and selectivity. The formation energies of monatomic O and Cu-defects on the CuO(111):Cu/O surface were obtained as 2.58 and 2.68 eV, respectively. Thus, in order to examine the impact of defects for nitrogen reduction reaction on CuO(111):Cu/O, a detailed evaluation with monatomic oxygen and copper defects has been carried out. The surfaces and corresponding energy diagrams involved in the reduction of N_2 to NH_3 are provided in the following.

Oxygen Defect. Oxygen defects have been created by removing a 3-fold coordinated O_{3K} atom from the CuO(111):Cu/O surface. As expected, a relaxation of the atoms surrounding the defective site is noticed. Hence, there is a mixture of coordinatively saturated and unsaturated sites of Cu as well as O on the surface (cf. Figure 10). Apart from changing the coordination environment, this defect also alters the electronic and magnetic properties of the surface.

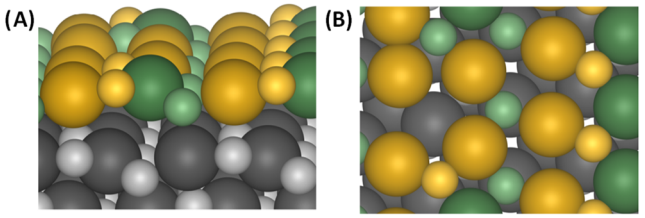

Figure 10. (A) Side and (B) top views of CuO(111):Cu/O with an O-defect. The larger and smaller spheres depict Cu and O atoms, correspondingly. Based on the coordination numbers, the atoms are colored yellow (CN = 3) and green (CN = 4), respectively.

Similar to the previous sections, the energy profile of the NRR intermediates on the O-defective CuO(111):Cu/O, along different pathways, is furnished in Figure 11. Also, the

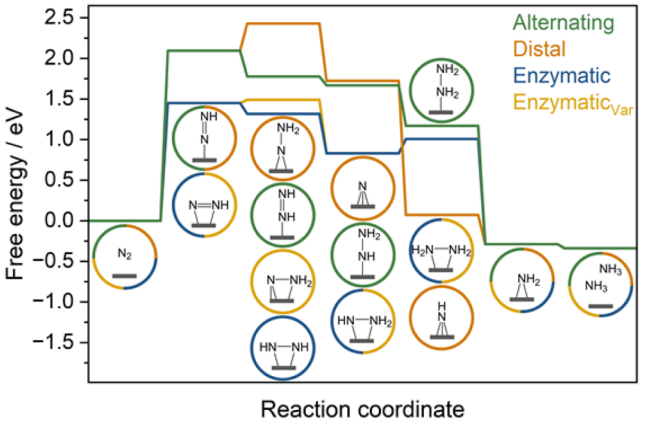

Figure 11. Free energy profiles for various NRR mechanisms on O-deficient CuO(111):Cu/O.

individual mechanisms with corresponding structures are showcased in Figure S4A−D. Also, each intermediate was adsorbed in plausible positions at the surface of interest, with the energetically stable structures chosen for further evaluation. Here, *NNH adsorbs directly at the defective O site, where one of the N atoms occupies the vacant site and is bound to three Cu atoms, whereas the other N atom forms a Cu−N contact with one of the Cu atoms. As observed for all of the cases discussed in the previous sections, the first hydrogenation step serves as the limiting one for NRR with an energy of 2.10 and 1.45 eV for alternating/distal and enzymatic/enzymatic$_{var.}$ mechanisms, respectively. A considerable energy difference of 0.65 eV between the singly- and doubly bound N atoms to the surface showcases the escalated viability in the onset of enzymatic and enzymatic$_{var.}$ mechanisms, with respect to the initial reduction step. In the second hydrogenation step, intermediate *NHNH binds to the surface with both N atoms (enzymatic/enzymatic$_{var.}$) over the O-defect site. This configuration is clearly preferred over the intermediates bound to the surface with a single N atom (alternating/distal). Similar to the previous step, *$NHNH_2$ (as described by

https://doi.org/10.1021/acs.jpcc.5c03667
J. Phys. Chem. C 2025, 129, 15978−15990

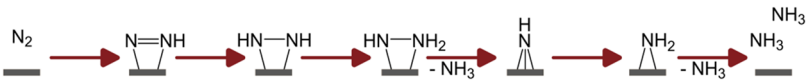

Figure 12. Schematic representation of the thermodynamically preferred NRR mechanism on CuO(111):Cu/O with an O vacancy.

the enzymatic mechanism) prefers adsorbing at an O-defect site for the third hydrogenation step. Moreover, the fourth hydrogenation pertaining to the enzymatic and enzymatic$_{var.}$ mechanisms is highly endergonic, whereas the *NH intermediate of the distal mechanism adsorbed directly at the defective site generates a free energy of −1.65 eV. In general, the intermediates on the O-deficient CuO(111):CuO either prefer adsorbing at or over the defect site. Moreover, the bridge position between two coordinatively unsaturated Cu atoms at the O-defect site is preferred by the *NH_2 intermediate. These observations pertaining to the intermediates not preferring to be adsorbed directly in the defective sites rule out the probability of a Mars−van Krevelen mechanism on the O-defective CuO(111):Cu/O. Summarizing the previous observations, the thermodynamically favored pathway for NRR on the O-defective surface has been derived and furnished in Figure 12. NRR on this surface follows the enzymatic pathway with a limiting potential of −1.45 V (cf. Figure S2C) only with an exception in the *NH intermediate formation, where the distal mechanism is energetically more viable. Also, it is conspicuous that except for the first hydrogenation fraction, the free energies of all of the other steps following enzymatic and distal pathways up until NH_3 formation are downhill and exergonic.

Copper Defect. Cognizance of the NRR mechanism on the copper defective CuO(111):Cu/O surface is realized by the removal of a Cu atom (Cu_{3K-}) and subsequent relaxation of the surface (cf. Figure 13). In this, the three oxygen atoms

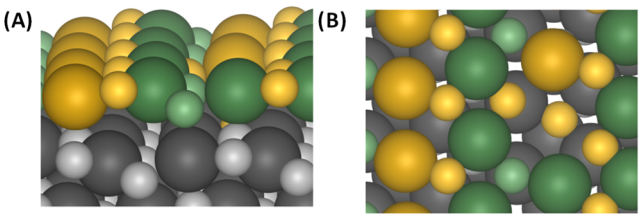

Figure 13. (A) Side and (B) top views of the Cu-defective CuO(111):Cu/O surface. The larger and smaller spheres represent Cu and O atoms, respectively. Atoms with coordination numbers three and four are designated as yellow and green-colored balls, correspondingly.

that were bound to the removed Cu_{3K-} atom are found to be coordinatively unsaturated. Hence, to compensate for the absence of Cu−O bonds, O atoms engage in bonding interactions with the neighboring Cu_{3K} atom, thereby altering its coordination number to four and making it coordinatively saturated. Thus, the Cu-defective surface comprises coordinatively saturated and unsaturated sites, as indicated in Figure 13. Apart from influencing the outermost surface layer, the Cu-defect also influences second-layer atoms, owing to the coordinatively unsaturated O atom, which is located exactly beneath the Cu_{3K-} defect. In addition to this, it affects the magnetic behavior of atoms at the surface, in particular for Cu atoms adjacent to the defect, whereas the magnetic properties of all other Cu atoms remain (almost) unchanged.

With reference to the previous sections, the adsorption of various NRR intermediates was explored on CuO(111):Cu/O with a Cu-defect. The stability of the intermediates was scrutinized by adsorbing it at various sites, and the one that required the lowest energy was considered for further calculations. Also, the free energy diagrams of the intermediates along various pathways are displayed in Figure 14.

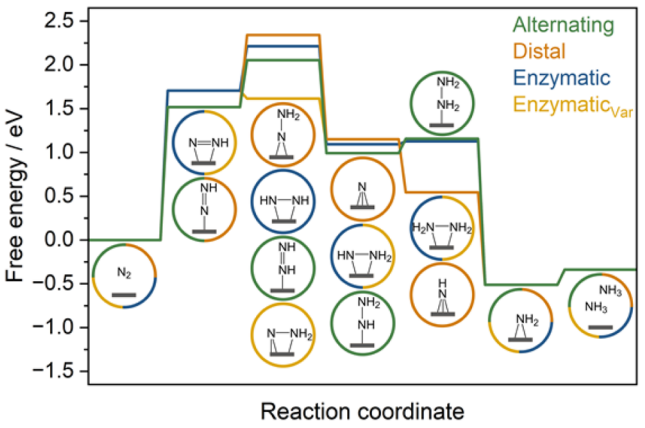

Figure 14. Free energy profiles of multifarious mechanisms involved in NRR on the CuO(111) surface with a Cu-defect.

Besides, the individual mechanisms, along with the adsorption structures, are furnished in Figure S5A−D. Again, the first hydrogenation step is strongly endergonic and appears to be the limiting step along the NRR on Cu-deficient CuO(111):Cu/O. The free energies recorded for the alternating/distal and enzymatic/enzymatic$_{var.}$ mechanisms are 1.52 and 1.71 eV, respectively. The alternating/distal pathway favors the adsorption of *NNH rather than the enzymatic/enzymatic$_{var.}$ mechanism, as observed for O-defects. The second reduction step is energetically favored only along the enzymatic$_{var.}$ mechanism (where both H atoms are attached to the same N, *NNH_2). In the third hydrogenation step, all free energy values are almost equivalent, but the most preferred pathway turned out to be the alternating one.

Further, the fourth hydrogenation proceeds via the distal pathway, which is analogous to that noticed for the surface with O-defects. Similar to the reconstructed surface, the final hydrogenation step resulting in NH_3 is slightly higher in energy than the *NH_2 intermediate formation. Interestingly, a combination of alternating, enzymatic$_{var.}$, and distal pathways drives nitrogen reduction reactions on this surface (see Figure 15), and the limiting potential required for this pathway amounted to −1.52 V (cf. Figure S2D). Under reaction conditions detailed for NRR on CuO by Wang *et al.*[18] and Han *et al.*,[46] the reduction of Cu might take place. However, the plausibility of Cu leaching into the solution as a solvated ion can be anticipated to be minimal. Nevertheless, unsaturated Cu^{2+} ions at the grain boundary and edge sites might interact with SO_4^{2-} ions, thereby aiding their dissolution. Further, in the context of plasma catalysis, there are literature reports that support the reduction of Cu_2O to its metallic state,[47] Cu which will be oxidized to Cu^{2+} and form a solvation complex with

https://doi.org/10.1021/acs.jpcc.5c03667
J. Phys. Chem. C 2025, 129, 15978−15990

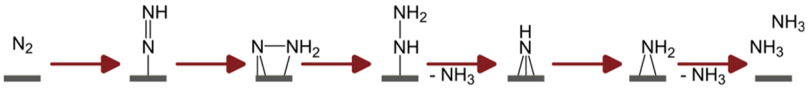

Figure 15. Schematic representation of energetically favorable individual intermediates contributing to the thermodynamic mixed pathway for the reduction of nitrogen on Cu-defective CuO(111):Cu/O.

SO_4^{2-} ion, that would foster its dissolution. This formed the reason for investigating the role of Cu vacancies in the NRR to ensure completeness.

Strategic Insights on the Examined Surfaces: A Focus on NRR Efficiency. The considered CuO(111) surfaces exhibit a variety of active centers and hence follow different pathways during the course of reduction to NH_3. In order to elucidate the response of the different surfaces, we exemplarily compared the interaction of *NNH as well as changes in the surface structure during adsorption and desorption (see Figure 16).

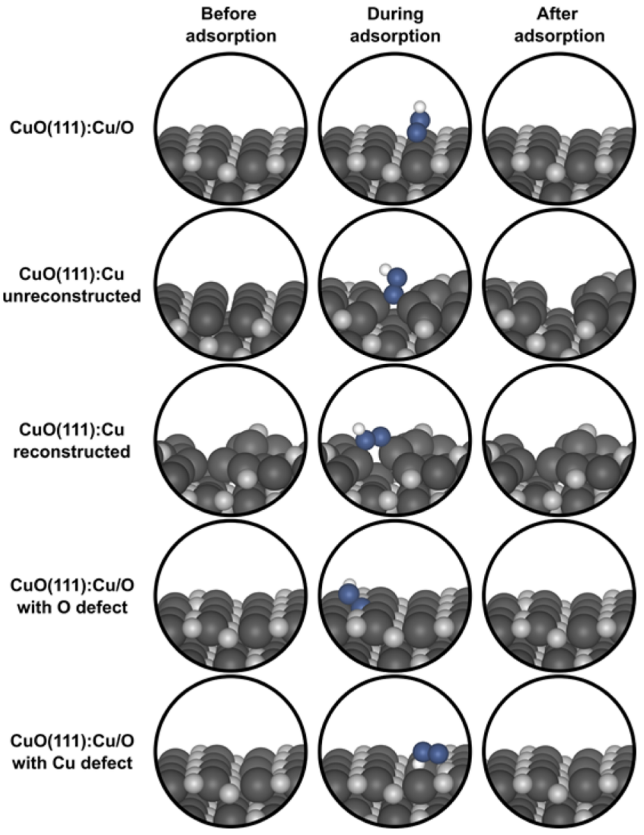

Figure 16. Surface structure of CuO(111):Cu/O, the unreconstructed and reconstructed CuO(111):Cu, as well as CuO(111):Cu/O with monatomic oxygen and copper defects before, during adsorption, and after desorption of *NNH.

The CuO(111):Cu/O surface does not show structural rearrangements upon adsorption and consecutive desorption of *NNH. Although the surface displays a slight relaxation for the adsorption of individual intermediates such as atomic N, the initial structure of the surface was always restored after the respective desorption, an aspect that was also observable for all other intermediates on CuO(111):Cu/O.

Conversely, the adsorption of intermediates led to certain reconstructions on the Cu-terminated CuO(111):Cu surface. The relaxed structure after desorption of *NNH exhibited structural and energy variations in comparison to the unreconstructed surface before adsorption. This observation directly implies that the unreconstructed CuO(111):Cu surface is not being restored after the adsorption and desorption of *NNH. Thus, this surface seems not suitable for estimating the free energy profile as well as thermodynamic feasibility since the stability is questionable. Moreover, a significant relaxation of the surface was observed during the adsorption of the *NNH intermediate on reconstructed CuO(111):Cu, which relaxes back to its original structure during *NNH desorption. Therefore, evaluating the thermodynamic behavior of the system is more reasonable on the reconstructed surface than on the metastable, unreconstructed one. Furthermore, the Cu/O-defective CuO(111):Cu/O surfaces also showed a restoration of the surface morphology after desorption of *NNH. Thus, overall, only the unreconstructed CuO(111):Cu surface showed an altered behavior.

The presence of diverse active centers on these surfaces is responsible for the variations in the stabilization of intermediates. Thus, the different surface sites influence the course of reduction from N_2 to NH_3 via various thermodynamic pathways. Since the individual mechanisms pertaining to each surface have been elaborated in the previous sections, the following discussion solely focuses on comparing and highlighting the similarities as well as differences.

The first distinction is the enormous variation in free energies recorded with respect to the first hydrogenation step for the individual mechanisms. It is well evidenced that CuO(111):Cu/O required a rather high energy of 2.58 eV for the first reduction step, whereas reconstructed CuO(111):Cu, as well as O- or Cu-defective CuO(111):Cu/O, show similar values of 1.41, 1.45, and 1.52 eV, respectively. The pristine CuO surface is known for its lower faradaic efficiency and ammonia yield, which is also reflected by its high activation energy barrier of 2.58 eV, which is in agreement with the literature value of 2.22 eV.[46] This behavior can be explained with the large concentration of defects as well as coordinatively unsaturated sites (low-coordinated Cu atoms) available on the other surfaces, which facilitated efficient bond formation between the surface and the adsorbate. Thus, this acted as the driving force for the onset of hydrogenation reactions at lower energies, in comparison to the CuO(111):Cu/O surface.

Thermodynamically favored mechanisms for individual surfaces vary from each other during the second hydrogenation reaction. The intermediates adsorbed on all of the surfaces are different, each corresponding to one of the four mechanisms investigated. For the third hydrogenation step, the $*NH_2NH$ intermediate of the alternating pathway predominates for all of the surfaces, with an exception of O-defective substrates, where the enzymatic intermediate with doubly bound N atoms was found to be more favored. Moreover, in the fourth reduction step, it is conspicuous that one of the NH_3 molecules splits off, leaving behind the *NH intermediate of the distal mechanism for the reconstructed and defective surfaces. In contrast to this, the formation of the $*NH_2NH_2$ intermediate of the enzymatic mechanism is thermodynamically more favored for

https://doi.org/10.1021/acs.jpcc.5c03667
J. Phys. Chem. C 2025, 129, 15978−15990

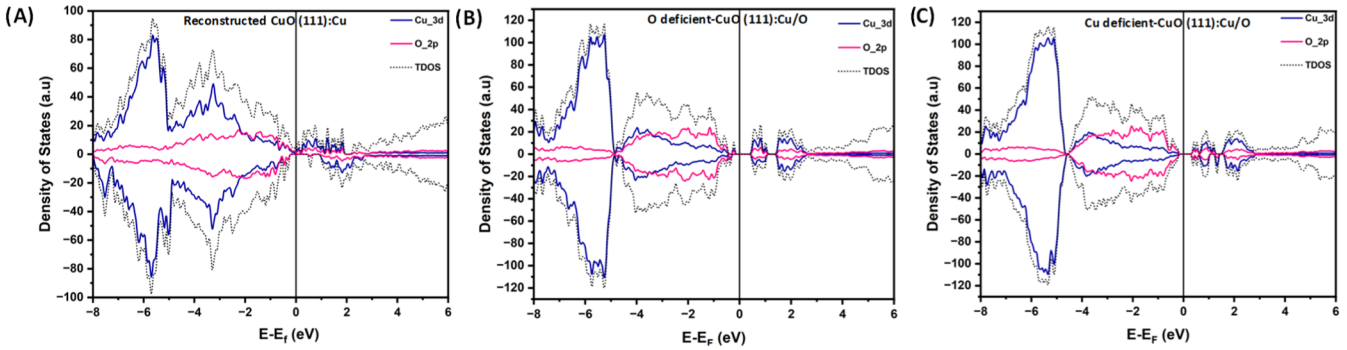

Figure 17. PDOS plots of (A) pristine CuO(111):Cu/O, (B) CuO(111):Cu, and (C) O-defective CuO(111):Cu/O surfaces before the adsorption of the *NNH intermediate.

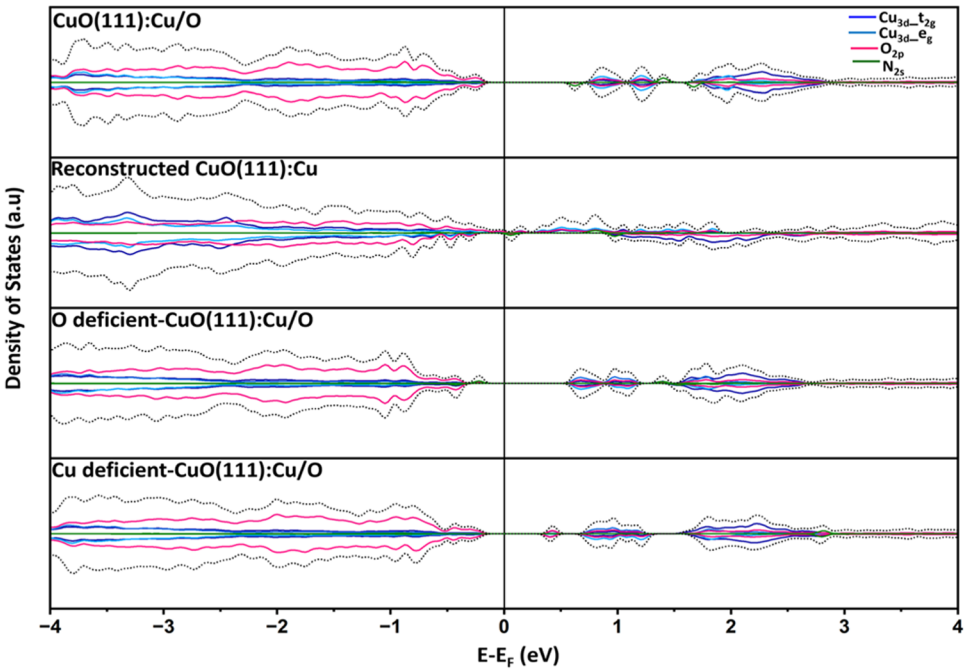

Figure 18. PDOS shows the surfaces of interest. The black dotted line in the up and down-spin states corresponds to the total density of states.

CuO(111):Cu/O. The possible explanation for this behavior would be that the distal mechanism offers strong binding and stabilization of the intermediates in the former surfaces by reducing the free energies and shifting the endergonic processes to exergonic ones. Conversely, for the defect-free surface, the splitting of NH_3 resulting in adsorbed *NH was found to be highly endergonic, yielding a free energy value of 1.8 eV. The fifth reduction step, resulting in the formation of *NH_2 for all of the surfaces, is identical, with N being adsorbed between two Cu atoms. In the final reduction step from N_2 to NH_3, it was evidenced that the process is exergonic for CuO(111):Cu/O as well as O-defective surfaces, whereas for the remaining ones, it is endergonic.

Overall, it can be seen that alternating and enzymatic pathways are favored on the CuO(111):Cu/O surface. Meanwhile, for the surface with O-defects, the enzymatic pathway is preferent. Unlike the above-mentioned substrates, the reconstructed and Cu-defective surfaces were found to favor different intermediates of the four-reaction mechanism and followed a mixed pathway. In addition, Nguyen *et al.* observed that the first hydrogenation step for NRR on hematite surfaces demanded a higher energy, and this differed depending on the surface terminations of each iron oxide substrate.[48] This trend also holds true for the CuO(111) surfaces explored in the current study.

Second, the electronic structures before hydrogenation of the four different surfaces of interest are analyzed via the PDOS plots (cf. Figure 17). In the case of the pristine CuO(111):Cu/O surface, a band gap of about 1.2 eV can be observed.[21] Interestingly, for the reconstructed surface, the up-spin state is conducting, whereas the down-spin state records a gap of 0.56 eV. Thus, this surface exhibits half-metallicity, a phenomenon attributable to the surface adopting an almost linear O−Cu−O arrangement as in the Cu_2O-bulk phase. In general, half-metallic behavior has been documented in Cu_2O for specific surfaces.[49] In contrast, the unreconstructed surface is characterized by an absence of the forbidden energy gap for both spin directions.[21] Although both the reconstructed and unreconstructed surfaces feature 2-fold coordinated Cu atoms in an O−Cu−O arrangement, the latter displays a higher concentration of 4-fold coordinated Cu atoms than the former. Besides, for the O-defective surface, energy gaps of 0.44 and 0.55 eV for the up and down-spin states are noticed, respectively. Further, the Cu-deficient surface records a band

https://doi.org/10.1021/acs.jpcc.5c03667
J. Phys. Chem. C 2025, 129, 15978−15990

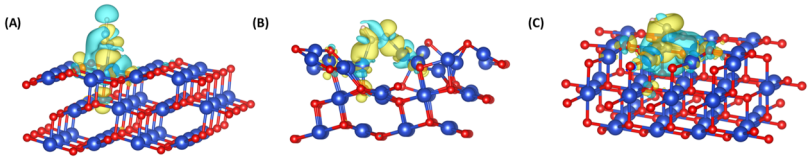

Figure 19. Charge density difference plots of *NNH adsorbed on (A) CuO(111):Cu/O, (B) CuO(111):Cu and (C) the O-defective surface. The blue, red, gray, and pink spheres represent Cu, O, N, and H atoms, respectively. For all plots, the isosurface level was chosen at 0.00059 e/Å^3.

gap of 0.35 and 0.30 eV in the up- and down-spin states, respectively. Apart from the pristine surface, all of the others exhibit a nonzero total magnetic moment value, which is reflected from the asymmetric shape of the spin-up and -down states in the PDOS plots, resulting in a certain degree of spin polarization.

Similarly, we have furnished the PDOS plots to showcase the hybridization persisting between *NNH and the CuO(111) substrate for the initial hydrogenation reaction (Figure 18). The PDOS plots of the pristine surface before and during adsorption of *NNH are quite similar. Compared to the pristine surface, which has states at 1.3 eV in the conduction band minimum, here N−2*p* states can be found at 0.62 and 1.4 eV, below the 3*d* states of Cu (cf. Figure 18). Meanwhile, the introduction of N−2*p* states reduces the band gap, but the shape of the up- and down-spin states differs from the former, showcasing the existence of spin polarization, which is also supported by its total magnetic moment value. Further, hybridization persisting between Cu−3*d* and N−2*p* states can also be seen from the charge density difference plots (CDDP) between Cu and N atoms (cf. Figure 19A) as well as from the Bader charge gained by nitrogen that binds to a Cu, which amounts to −0.11 e.

In the case of the reconstructed surface, it can be seen that *NNH adsorption results in a spike in the conductivity along both spin directions. The hybridization brought about by 3*d* states of Cu with 2*p* states of N can be evidenced at the Fermi level of the spin-down DOS. Also, orbital overlap between the states of O−2*p* with that of Cu−3*d* states is observed at the Fermi level. All of these orbital overlaps are responsible for the closure of the energy gap at the spin-down states of the bare reconstructed surface. Besides, nitrogen, which is bound to Cu, has gained a charge of −0.25e, and the other nitrogen that is bound to both Cu and H has received −1.07 e to preferentially bind to O atoms rather than Cu atoms. The band gap of the up- and down-spin states of this surface amounts to 0.38 and 0.36 eV, which does not differ much from that of the bare surface.[50] Hence, from all of these studies, it becomes clear that Cu engages in a very strong interaction with N in the case of the reconstructed and O-defective surfaces. The enhanced charge-gain and bonding characteristics between Cu−3*d* and N−2*p* orbitals in the O-defective surface establish it as a conducive one for NRR. This bonding interaction between Cu and N might weaken the N═N bonding in the *NNH intermediate, thereby activating it for the production of NH_3. This can be validated by obtaining the bond strength values from ICOHP plots, which are discussed in the following section.

The Integrated Crystal Hamilton Population (ICOHP) analysis for free N_2 in vacuum yielded an ICOHP value of −23.4, and this aligns well with the literature value of −23.0.[51] Bond strength values of N−N interactions for the four surfaces during the initial hydrogenation reaction are shown in Table 1, where more negative ICOHP values indicate stronger bonds.

Table 1. Considered Surfaces along with Their ICOHP Values for the N−N Interaction in the *NNH Intermediate

surface	ICOHP value
pristine CuO(111):Cu/O	−20.01
reconstructed CuO(111):Cu	−18.06
O-defect on CuO(111):Cu/O	−15.15
Cu-defect on CuO(111):Cu/O	−18.54

Among the surfaces, the pristine one recorded the lowest value of −20.01, while the O-deficient surface had the highest value at −15.15, making it the most favorable for *NNH formation due to a significant weakening of the N≡N triple bond. Thus, the ICOHP plots reveal an increase in antibonding interactions in the O-defective surface, which aids the activation of the inert N≡N bond (cf. Figure S6). In addition, there are four Cu−N interactions on the O-defective surface with ICOHP values of −2.83, −3.26, −2.62, and −3.00, compared to just one interaction of −3.65 for CuO(111):Cu/O. This highlights the enhanced Cu−N and weakened N≡N interactions on the O-deficient surface, critical for accelerating the NRR.

Thus, a systematic ICOHP analysis of the other NRR intermediates on the O-defective surface was performed. Here, the N−N interaction in *NHNH and *NH_2NH increases to −13.66 and −9.98, thereby indicating a weakening of the bond. Additionally, one Cu−N interaction surges from −3.95 (in *NHNH) to −2.82 (in *NH_2NH), facilitating the splitting of the first NH_3 unit during the consecutive hydrogenation. The ICOHP values of −3.12, −3.28, and −3.93 indicate strong Cu−N interactions in *NH, while *NH_2 exhibits interactions of −3.27 and −3.28, after which the second NH_3 unit is detached due to successive hydrogenation.

Summary and Perspectives. In this work, we have studied the NRR on different CuO(111) surfaces, providing important information on preferential reaction sites, thermodynamic feasibility, as well as the overall reaction mechanisms. Here, it is conspicuous that N prefers adsorbing on either coordinatively unsaturated Cu or defect sites. With regard to the pathway, it can be seen that different surfaces stabilize the intermediates to different degrees owing to the plethora of various sites available on the substrate. The surfaces follow a mixed-type pathway rather than one mechanism, emerging to be the most favorable for all of the surfaces. The reconstructed surface and the one with an O-defect yielded the lowest free energies of 1.41 and 1.45 eV, which conforms with the limiting potentials for these two surfaces of −1.41 and −1.45 V, respectively. Further, it was found that hydrogenation steps were all exergonic on CuO(111):Cu/O with O-defects, while the preferred mechanism for the NRR on the reconstructed surface comprises endergonic hydrogenation steps. Besides, the surface with oxygen defects possesses well-defined active centers at the defect sites, while the Cu−terminated CuO(111):Cu surface has several coordinatively unsaturated Cu atoms and thus several active centers on the surface, but

https://doi.org/10.1021/acs.jpcc.5c03667
J. Phys. Chem. C 2025, 129, 15978−15990

this surface is also susceptible to irreversible structural changes during the reaction. Overall, our investigations indicate CuO(111):Cu/O with O-defects to be particularly promising for the nitrogen reduction reaction.

Also, the strong hybridization that exists between Cu−3*d* and N−2*p* states at the O-deficient surface facilitates the formation of Cu−N bonds with an accumulation of negative charge at the nitrogens. Unlike the reconstructed surface, the ICOHP value of N≡N interactions on O-defective surfaces emerged as −15.15, which signified an activation of the triple bond of N_2. In addition, the antibonding contributions of N−N interactions on the O-defective surface are higher than those for the other surfaces, thereby showcasing a pronounced weakening of the N≡N triple bond. Besides, decreasing bond strength with further hydrogenation steps conferred the O-defective surface as the most desirable surface for NRR. This work furnishes a detailed description of structural and electronic aspects of CuO(111) surfaces and highlights the influence of the O vacancy on NRR. Further, computational and experimental studies are necessary to account for electrochemical effects such as pH, potential, and solvation, thereby enabling a realistic description of vacancy formation as well as the overall reaction pathways. Thus, the current study might serve as an impetus for experimental studies to design and tune the morphology of CuO structures to achieve enhanced catalytic efficiency for NH_3 production under ambient conditions.

■ ASSOCIATED CONTENT

Data Availability Statement

The data supporting the findings of this study are openly available in Zenodo at 10.5281/zenodo.16374131.

Supporting Information

The Supporting Information is available free of charge at https://pubs.acs.org/doi/10.1021/acs.jpcc.5c03667.

The data that supports the research findings furnished here can be found in the Supporting Information of this article, including optimized configurations, adsorption energies, limiting potential of various surfaces, free energy plots, along with intermediate structures along four pathways, as well as ICOHP plots (PDF)

■ AUTHOR INFORMATION

Corresponding Author

Timo Jacob − *Institute of Electrochemistry, Ulm University, 89081 Ulm, Germany; Helmholtz−Institute Ulm (HIU) Electrochemical Energy Storage, 89081 Ulm, Germany; Karlsruhe Institute of Technology (KIT), 76021 Karlsruhe, Germany;* orcid.org/0000-0001-7777-2306; Email: timo.jacob@uni-ulm.de

Authors

Stefanie E. Bogenrieder − *Institute of Electrochemistry, Ulm University, 89081 Ulm, Germany;* orcid.org/0009-0006-9201-4486

C. Hepsibah Priyadarshini − *Institute of Electrochemistry, Ulm University, 89081 Ulm, Germany; Helmholtz−Institute Ulm (HIU) Electrochemical Energy Storage, 89081 Ulm, Germany; Karlsruhe Institute of Technology (KIT), 76021 Karlsruhe, Germany;* orcid.org/0000-0001-7096-4217

Julian Beßner − *Institute of Electrochemistry, Ulm University, 89081 Ulm, Germany;* orcid.org/0000-0001-9454-3679

Complete contact information is available at: https://pubs.acs.org/10.1021/acs.jpcc.5c03667

Author Contributions

The manuscript was written through the contribution of all authors. S.E.B. and C.H.P. contributed equally to the work. J.B: analysis, review, and editing. T.J.: resources, supervision, and writing—review and editing. All authors have given approval to the final version of the manuscript.

Author Contributions

‖S.E.B. and C.H.P contributed equally to this work.

Notes

The authors declare no competing financial interest.

■ ACKNOWLEDGMENTS

The authors acknowledge support from the state of Baden-Württemberg through bwHPC and the German Research Foundation (DFG) through Grant No. INST 40/575-1 FUGG (JUSTUS 2 cluster). Additional simulations were performed on the high-performance computing cluster ULMIX provided by the Institute of Electrochemistry at Ulm University. Further, support from the DFG through the priority program SPP-2370 (project 502202153) and the collaborative research centre SFB-1316 (project 327886311) is gratefully acknowledged.

■ REFERENCES

(1) Liu, D.; Chen, M.; Du, X.; Ai, H.; Lo, K. H.; Wang, S.; Chen, S.; Xing, G.; Wang, X.; Pan, H. Development of Electrocatalysts for Efficient Nitrogen Reduction Reaction under Ambient Condition. *Adv. Funct. Mater.* **2021**, *31*, No. 2008983.

(2) Shipman, M. A.; Symes, M. D. Recent Progress towards the Electrosynthesis of Ammonia from Sustainable Resources. *Catal. Today* **2017**, *286*, 57−68.

(3) Giddey, S.; Badwal, S.; Kulkarni, A. Review of Electrochemical Ammonia Production Technologies and Materials. *Int. J. Hydrogen Energy* **2013**, *38* (34), 14576−14594.

(4) Li, S. J.; Bao, D.; Shi, M. M.; Wulan, B. R.; Yan, J. M.; Jiang, Q. Amorphizing of Au Nanoparticles by CeOx−RGO Hybrid Support towards Highly Efficient Electrocatalyst for N_2 Reduction under Ambient Conditions. *Adv. Mater.* **2017**, *29*, No. 1700001.

(5) Huang, H.; Xia, L.; Shi, X.; Asiri, A. M.; Sun, X. Ag Nanosheets for Efficient Electrocatalytic N_2 Fixation to NH_3 under Ambient Conditions. *Chem. Commun.* **2018**, *54*, 11427−11430.

(6) Kitano, M.; Kanbara, S.; Inoue, Y.; Kuganathan, N.; Sushko, P. V.; Yokoyama, T.; Hara, M.; Hosono, H. Electride Support Boosts Nitrogen Dissociation over Ruthenium Catalyst and Shifts the Bottleneck in Ammonia Synthesis. *Nat. Commun.* **2015**, *6*, No. 6731.

(7) Danish, M. S. S. Exploring Metal Oxides for the Hydrogen Evolution Reaction (HER) in the Field of Nanotechnology. *RSC Sustainable* **2023**, *1*, 2180−2196.

(8) Song, F.; Bai, L.; Moysiadou, A.; Lee, S.; Hu, C.; Liardet, L.; Hu, X. Transition Metal Oxides as Electrocatalysts for the Oxygen Evolution Reaction in Alkaline Solutions: An Application−Inspired Renaissance. *J. Am. Chem. Soc.* **2018**, *140* (25), 7748−7759.

(9) Iwama, R.; Takizawa, K.; Shinmei, K.; Baba, E.; Yagihashi, N.; Kaneko, H. Design and Analysis of Metal Oxides for CO_2 Reduction Using Machine Learning, Transfer Learning, and Bayesian Optimization. *ACS Omega* **2022**, *7* (12), 10709−10717.

(10) Lee, C. H.; Pahari, S.; Sitapure, N.; Barteau, M. A.; Kwon, J. S. Investigating High−Performance Non−Precious Transition Metal Oxide Catalysts for Nitrogen Reduction Reaction: A Multifaceted DFT−kMC−LSTM Approach. *ACS Catal.* **2023**, *13*, 8336−8346.

(11) Zoolfakar, A. S.; Rani, R. A.; Morfa, A. J.; O'Mullane, A. P.; Kalantar−Zadeh, K. Nanostructured Copper Oxide Semiconductors: A Perspective on Materials, Synthesis Methods and Applications. *J. Mater. Chem. C* **2014**, *2*, 5247−5270.

(12) Giziński, D.; Brudzisz, A.; Santos, J. S.; Trivinho−Strixino, F.; Stępniowski, W. J.; Czujko, T. Nanostructured Anodic Copper Oxides as Catalysts in Electrochemical and Photoelectrochemical Reactions. *Catalysts* **2020**, *10*, 1338.
(13) Rydosz, A. The Use of Copper Oxide Thin Films in Gas−Sensing Applications. *Coatings* **2018**, *8*, 425.
(14) Majumdar, D.; Ghosh, S. Recent Advancements of Copper Oxide−Based Nanomaterials for Supercapacitor Applications. *J. Energy Storage* **2021**, *34*, No. 101995.
(15) Chakraborty, N.; Banerjee, J.; Chakraborty, P.; Banerjee, A.; Chanda, S.; Ray, K.; Acharya, K.; Sarkar, J. Green Synthesis of Copper/Copper Oxide Nanoparticles and Their Applications: A Review. *Green Chem. Lett. Rev.* **2022**, *15*, 187−215.
(16) Sumanth, A.; Mishra, V.; Pandey, P.; Rao, M. S. R.; Dixit, T. Investigations into the Role of Native Defects on Photovoltaic and Spintronic Properties in Copper Oxide. *IEEE Trans. Nanotechnol.* **2022**, *21*, 522−527.
(17) Jang, Y. J.; Lindberg, A. E.; Lumley, M. A.; Choi, K.−S. Photoelectrochemical Nitrogen Reduction to Ammonia on Cupric and Cuprous Oxide Photocathodes. *ACS Energy Lett.* **2020**, *5* (6), 1834−1839.
(18) Wang, F.; Liu, Y.−P.; Zhang, H.; Chu, K. CuO/Graphene Nanocomposite for Nitrogen Reduction Reaction. *ChemCatChem* **2019**, *11* (5), 1441−1447.
(19) Zanling, H.; Madiha, R.; Reda, W. A.; Tong, Q.−X.; Astruc, D.; Hu, L. Recent Progress in Electrocatalytic Nitrogen Reduction to Ammonia (NRR). *Coord. Chem. Rev.* **2023**, *478*, No. 214981.
(20) Mishra, A. K.; Roldan, A.; de Leeuw, N. H. CuO Surfaces and CO_2 Activation: A Dispersion−Corrected DFT+U Study. *J. Phys. Chem. C* **2016**, *120* (4), 2198−2214.
(21) Bogenrieder, S. E.; Beßner, J.; Engstfeld, A. K.; Jacob, T. First−Principles Study on the Structural and Magnetic Properties of Low−Index Cu_2O and CuO Surfaces. *J. Phys. Chem. C* **2024**, *128* (23), 9693−9704.
(22) Bogenrieder, S. E. Theoretical Investigations on Nitrogen Reduction on Copper Oxide Surfaces. In *Dissertation*; Ulm University, 2024.
(23) Kresse, G.; Furthmüller, J. Efficiency of Ab−Initio Total Energy Calculations for Metals and Semiconductors Using a Plane−Wave Basis Set. *Comput. Mater. Sci.* **1996**, *6*, 15−50.
(24) Kresse, G.; Furthmüller, J. Efficient Iterative Schemes for Ab−Initio Total−Energy Calculations Using a Plane−Wave Basis Set. *Phys. Rev. B* **1996**, *54*, 11169−11186.
(25) Blöchl, P. E. Projector Augmented−Wave Method. *Phys. Rev. B* **1994**, *50*, 17953−17979.
(26) Perdew, J. P.; Burke, K.; Ernzerhof, M. Generalized Gradient Approximation Made Simple. *Phys. Rev. Lett.* **1996**, *77*, 3865−3868.
(27) Dudarev, S. L.; Botton, G. A.; Savrasov, S. Y.; Humphreys, C. J.; Sutton, A. P. Electron−Energy−Loss Spectra and the Structural Stability of Nickel Oxide: An LSDA+U Study. *Phys. Rev. B* **1998**, *57*, 1505−1509.
(28) Živković, A.; Roldan, A.; de Leeuw, N. H. Density Functional Theory Study Explaining the Underperformance of Copper Oxides as Photovoltaic Absorbers. *Phys. Rev. B* **2019**, *99*, No. 035154.
(29) Skúlason, E.; Bligaard, T.; Gudmundsdóttir, S.; Studt, F.; Rossmeisl, J.; Pedersen, F. A.; Vegge, T.; Jónsson, H.; Nørskov, J. K. A Theoretical Evaluation of Possible Transition Metal Electro−Catalysts for N_2 Reduction. *Phys. Chem. Chem. Phys.* **2012**, *14* (3), 1235−1245.
(30) Urrego−Ortiz, R.; Builes, S.; Calle−Vallejo, F. Impact of Intrinsic Density Functional Theory Errors on the Predictive Power of Nitrogen Cycle Electrocatalysis Models. *ACS Catal.* **2022**, *12*, 4784−4791.
(31) Urrego−Ortiz, R.; Builes, S.; Illas, F.; Calle−Vallejo, F. Gas−Phase Errors in Computational Electrocatalysis: A Review. *EES Catal.* **2024**, *2*, 157−179.
(32) Chase, M. J. NIST−JANAF Thermochemical Tables, Fourth Edition. *J. Phys. Chem. Ref. Data Monograph 9*, 1998, pp 1−1961.
(33) Bader, R. F. W. Atoms in Molecules. *Acc. Chem. Res.* **1985**, *18*, 9−15.
(34) Deringer, V. L.; Tchougréeff, A. L.; Dronskowski, R. Crystal Orbital Hamilton Population (COHP) Analysis as Projected from Plane−Wave Basis Sets. *J. Phys. Chem. A* **2011**, *115*, 5461−5466.
(35) Maintz, S.; Deringer, V. L.; Tchougréeff, A. L.; Dronskowski, R. LOBSTER: A Tool to Extract Chemical Bonding from Plane−Wave Based DFT. *J. Comput. Chem.* **2016**, *37*, 1030−1035.
(36) Hu, J.; Li, D.; Lu, J. G.; Wu, R. Effects on Electronic Properties of Molecule Adsorption on CuO Surfaces and Nanowires. *J. Phys. Chem. C* **2010**, *114*, 17120−17126.
(37) Wang, S.; Qian, C.; Zhou, S. Accelerating the Development of Electrocatalysts for Electrochemical Nitrogen Fixation through Theoretical and Computational Approaches. *Mater. Chem. Front.* **2023**, *7*, 4259−4280.
(38) Beßner, J.; Jacob, T. Understanding the Nitrogen Reduction Reaction Mechanism on $CuFeO_2$ Photocathodes. *Chem. - Eur. J.* **2025**, *31*, No. e202500058.
(39) Aubry, T. J.; Clary, J. M.; Miller, E. M.; Vigil-Fowler, D.; van de Lagemaat, J. Activating Nitrogen for Electrochemical Ammonia Synthesis via an Electrified Transition-Metal Dichalcogenide Catalyst. *J. Phys. Chem. C* **2024**, *128*, 7063−7072.
(40) Majumdar, P. Theory Investigations of Metal/Oxide Interfaces andTransition Metal Catalysts; Ph.D. Thesis, Purdue University Graduate School: West Lafayette, IN, 2021.
(41) Peng, P.; Schiappacasse, C.; Zhou, N.; Addy, M.; Cheng, Y.; Zhang, Y.; Ding, K.; Wang, Y.; Chen, P.; Ruan, R. Sustainable Non-Thermal Plasma-Assisted Nitrogen Fixation-Synergistic Catalysis. *ChemSusChem* **2019**, *12*, 3702−3712.
(42) Winter, L. R.; Chen, J. G. N_2 Fixation by Plasma-Activated Processes. *Joule* **2021**, *5*, 300−315.
(43) Hong, J.; Prawer, S.; Murphy, A. B. Plasma Catalysis as an Alternative Route for Ammonia Production: Status, Mechanisms, and Prospects for Progress. *ACS Sustainable Chem. Eng.* **2018**, *6*, 15−31.
(44) Mehta, P.; Barboun, P.; Herrera, F. A.; Kim, J.; Rumbach, P.; Go, D. B.; Hicks, J. C.; Schneider, W. F. Overcoming Ammonia Synthesis Scaling Relations with Plasma-Enabled Catalysis. *Nat. Catal.* **2018**, *1*, 269−275.
(45) Rouwenhorst, K. H. R.; Kim, H.-H.; Lefferts, L. Vibrationally Excited Activation of N_2 in Plasma-Enhanced Catalytic Ammonia Synthesis: A Kinetic Analysis. *ACS Sustainable Chem. Eng.* **2019**, *7*, 17515−17522.
(46) Han, X.; Zhou, W.; Huang, X.; Yu, H.; Yang, F.; Chen, S.; Wang, J. Enhancing Electrocatalytic N_2 Reduction to NH_3 by Introducing Ni Heteroatoms into $NiCuO_x$ Electrocatalyst. *Catal. Sci. Technol.* **2024**, *14*, 3691−3698.
(47) Wang, L.; Yao, X.; Jana, S.; Zhou, Y.; Qin, C.; Shou, H.; Teng, Y.; Chen, N.; Zhang, L.; Singh, C. V.; Tan, Z.; Wu, Y. A. Interface Engineering and Oxygen Vacancies Derived from Plasma-Treated Cu_2O Synergistically Enhancing Electrocatalytic CO_2-to-C_2^+ Conversion. *J. Mater. Chem. A* **2024**, *12*, 12345−12356.
(48) Nguyen, M. T.; Seriani, N.; Gebauer, R. Nitrogen Electrochemically Reduced to Ammonia with Hematite: Density−Functional Insights. *Phys. Chem. Chem. Phys.* **2015**, *17* (22), 14317−14322.
(49) Soon, A.; Cui, X. Y.; Delley, B.; Wei, S. H.; Stampfl, C. Native Defect−Induced Multifarious Magnetism in Nonstoichiometric Cuprous Oxide: First−Principles Study of Bulk and Surface Properties of $Cu_{2-\delta}O$. *Phys. Rev. B* **2009**, *79*, No. 035205.
(50) Živković, A.; de Leeuw, N. H. Exploring the Formation of Intrinsic P−Type and N−Type Defects in CuO. *Phys. Rev. Mater.* **2020**, *4*, No. 074606.
(51) Hou, P.; Huang, Y.; Ma, F.; Zhu, G.; Zhang, J.; Wei, X.; Du, P.; Liu, J. Single−Atom Catalyst of TM@D−Silicene−An Effective Way to Reduce N_2 into Ammonia. *Phys. Chem. Chem. Phys.* **2022**, *24*, 3486−3497.

https://doi.org/10.1021/acs.jpcc.5c03667
J. Phys. Chem. C 2025, 129, 15978−15990